Paweł Ziółkowski[a][*], Michał Stajnke[a] and Paweł Jóźwik[b]

Modeling of a mixture flow of helium and methanol in thermocatalytic reactor and chemical reactions on the intermethallic phase of Ni₃Al

[a] Energy Conversion Department, Institute of Fluid Flow Machinery, Polish Academy of Sciences, 80-231 Gdansk, Fiszera 14, Poland

[b] Department of Advanced Materials and Technologies, Faculty of Advanced Technologies and Chemistry, Military University of Technology, Kaliskiego 2, 00-908 Warsaw, Poland

Abstract

In this paper, the specified issues that occurs in the numerical modeling of complex phenomena of chemical reactions intensified with forced fluid flow in the thermocatalytic reactor channels on the intermetallic phase of Ni_3Al are presented. Based on the example of flowing mixture containing helium contaminated by methanol in a horizontal microchannels, heated from the outside, received results of the experiment were shown and compared with computational fluid dynamize calculations. However, standard version of commercial code have been expanded by user defined functions. These extensions transformed the calculation mechanisms and algorithms of computational fluid dynamize codes adapting them for the micro-flow cases and increased chemical reactions rate on an interphase between fluid and solid. Results obtained on the way of numerical calculations were compared with experimental data receiving satisfactory compliance.

Keywords: CFD modeling; Numerical analysis; Methanol decomposition; Catalytic reactions

[*]Corresponding Author. Email adress: pziolkowski@imp.gda.pl

Nomenclature

A	–	surface, m^2
$A_{(\alpha)}$	–	pre-exponential factor
$C_{p(m)}$	–	specific molar heat capacity of component (m) at constant pressure, $J/(mol\,K)$
$C_{v(m)}$	–	specific molar heat capacity of component (m) at constant volume, $J/(mol\,K)$
c_m^+	–	rate of the mass component formation relative to a volume, $kg/s\,m^3$
c_p	–	specific heat capacity at constant pressure, $J/(kg\,K)$
c_v	–	specific heat capacity at constant volume, $J/(kg\,K)$
D_{mm}	–	coefficient of multicomponents diffusion, m^2/s
D_m^T	–	coefficient of temperature diffusion, $kg/(m\,s)$
d	–	diameter, m
$E_{(\alpha)}$	–	activation energy, J/mol
e_m^+	–	energy sources, W/kg
e_b	–	transmit power of the black body, W/m^2
f_m	–	inertia of component, m^2/s
g	–	specific energy radiation, $J/m^2 s$
g_m	–	external driving force of phase transition, m^2/s^3
H	–	enthalpy, J
h	–	specific enthalpy, J/kg
$K_{(\alpha)}^C$	–	equilibrium constant for αth reaction
$k_{(\alpha)}^f$	–	forward rate constant of the αth reaction
$k_{(\alpha)}^r$	–	reverse rate constant of the αth reaction
L	–	length, m
l_m	–	internal driving force of phase transition, m^2/s^3
l_s	–	slip length, m
$\dot{m}$	–	mass flow rate, kg/s
NS	–	number of components
p	–	pressure, $N/m^2 = Pa$
q	–	progression level of chemical reaction, $mol/m^3 s$
R	–	gas constant, $J/kg\,K$
R_u	–	universal gas constant ($R_u = 8.3146$), $J/(mol\,K)$
r_m	–	radiation sources, W/kg
S	–	entropy, J/K
S_m	–	source of component m, $S_m = c_m^+$, $kg/s\,m^3$
T	–	temperature, K
t	–	time, s
W	–	molecular weight of mixture, kg/mol
$\overline{W}$	–	average molecular weight, $kg/kmol$
W_m	–	molecular mass of component, kg/mol
X	–	mole fraction, mol/mol
$[X]$	–	Molar concentration, mol/m^3
Y	–	mass fraction, kg/kg
$\otimes$	–	dyadic multiplicator
$\perp$	–	normal to surface component

$\parallel$ –   parallel to surface component

Notation for tensor and vector quantities

$\vec{b}_m$	–	mass force of component m due to Earth gravitation
$\vec{d}_m$	–	diffusion vector of component m
$\overset{\leftrightarrow}{d}_m$	–	symmetric rate of deformation
$\vec{e}_i$	–	versor, where $i=x,\ y,\ z$
$\vec{g}_m$	–	mass forces of component m due to concentration difference
$\vec{h}_m$	–	balanced flux of X_m
$\overset{\leftrightarrow}{I}$	–	unit tensor (Gibbs' idemfactor)
$\vec{J}_m$	–	diffusion flux of mth diffusible component
$\vec{J}_m^t$	–	turbulent diffusive flux
$\overset{\leftrightarrow}{l}_m$	–	spatial gradients
$\overset{\leftrightarrow}{M}_m^+$	–	source of angular momentum
$\vec{m}_m^+$	–	momentum source
$\vec{n}$	–	normal vector
$\vec{q}$	–	molecular heat flux
$\vec{q}^D$	–	diffusion heat flux of the mixture
$\vec{q}^h$	–	heat flux of binary diffusivity
$\vec{q}^m$	–	irreversible mechanical energy flux
$\vec{q}^{rad}$	–	radiative heat flux of the mixture
$\vec{q}^t$	–	turbulent heat flux
$\overset{\leftrightarrow}{r}$	–	Reynolds' turbulent stress (momentum flux)
$\overset{\leftrightarrow}{t}$	–	total momentum flux
$\overset{\leftrightarrow}{t}_m$	–	Cauchy's momentum flux of component m
$\vec{v}_m$	–	velocity of component m
$\vec{v}$	–	barycentric velocity
$\vec{V}_m$	–	diffusion velocity
$\vec{x}_{\mathbf{m}}$	–	position of component m
$\vec{X}_{\mathbf{m}}$	–	starting position of component
$\overset{\leftrightarrow}{\tau}$	–	momentum flux of viscous stress
$\overset{\leftrightarrow}{\tau}_m$	–	momentum flux of viscous stress of component m
$\overset{\leftrightarrow}{\tau}^c$	–	total irreversible momentum flux
$\overset{\leftrightarrow}{\tau}^{dyf}$	–	momentum flux resulting from diffusion
$\overset{\leftrightarrow}{\tau}^{rad}$	–	momentum flux resulting from radiation
$\overset{\leftrightarrow}{\tau}^{trans}$	–	momentum flux from transpiration
$\overset{\leftrightarrow}{\omega}_m$	–	antisymmetric vorticity

Dimensionless numbers

Na – Navier number
Pr – Prandtl number
Re – Reynolds number

Greek symbols

α – absorption coefficient, 1/m
$\alpha_{m'}$ – thermal diffusion coefficient, kg/m s
α_{cat} – factor of influence of 'third body'
$\beta_{(\alpha)}$ – temperature exponent in the rate constant
γ – density of component of the mth species, kg/m^3
δ_{ij} – Kronecker's delta
ε – dissipation of kinetic energy of turbulence, m^{2}s^3
ϵ – specific internal energy, J/kg
ϵ_m^{form} – energy formation at reference temperature, J/kg
κ – isentropic exponent
λ – thermal conductivity, W/(m K)
λ_t – turbulent conductivity, W/(m K)
μ – dynamic viscosity, Pa s
μ' – coefficient of second viscosity of the mixture, Pa s
ν – surface viscosity, Pa s m
$\upsilon_{m(\alpha)}$ – stoichiometric matrix coefficient
ρ – mixture density, kg/m^3
τ_m – time of relaxation, s
ϕ_{mm} – the Wilke matrix
χ – coefficient the phase transition progress
χ_m^+ – source of configurational forces, W/m^3
$\dot{\chi}_m$ – rate of volume fraction expands (changes), 1/s
$\dot{\omega}_m$ – chemical production rate of the mth species, (kmol/m^{3}s)

Subscripts and superscripts

α – number of chemical reaction; specific chemical reaction
cat – catalytic
$cell$ – computational cell
ε – dissipation of kinetic energy of turbulence
i, j – direction used at finite volume method, $i, j = 1, 2, 3$ (structural mesh)
k – turbulent kinetic energy
m, m' – components of mixture, $m = 1, 2, 3 \ldots$
mm' – interaction of components of mixture $m \neq m'$
lam – laminar
T – temperature
t – total
$turb$ – turbulent

1   Introduction

The issue of air purification method of zero waste thermocatalytic elimination the chemical and biological pollutants and the process of thermocatalytic hydrocarbons degradation and decomposition is currently relevant and highly developed. Such solutions are known for thermocatalytic reactors in which the role of active element perform noble metals [1,2], vanadium and titanium compounds [3,4] or nickel-based materials [5,6]. Increasingly popular are the thermocatalytic reactions that provide conversion of methanol to hydrogen [5–9].

Nickel-based catalysts exhibit extremely high catalytic activity in methanol decomposition and promote the production of carbon nanostructures (mainly carbon nanotubes) [5] . One of the Ni-based, solid-state catalysts is Ni_3Al [1], which belongs to multifunctional materials, combining properties of both the constructional and functional materials. They are resistant to oxidation and corrosion, have a relatively low density and a relatively high melting point, and are relatively easy to form [5]. According to the literature, Ni_3Al intermetallic thin foils exhibit catalytic properties in hydrocarbon decomposition reactions [9,10]. It is known that, the relatively high temperature of maximum hydrocarbon conversion is the main disadvantage of this material [5]. However, the high temperature of the process can be used for placing regenerative heat exchanger behind the system [1]. Therefore, innovative and extremely promising become making thermocatalyst with thin strips/alloy foil based on intermetallic phase Ni_3Al produced according to technology works [1,9,10]. One example of alloy foil package based on intermetallic phase Ni_3Al rolled into a honeycomb is shown in Fig.1, where the thickness of Ni_3Al film is compared to the thickness of a human hair.

Appropriate dimensions of the device were selected in order to obtain complete decomposition of subtracts during contact time of the flow of the catalytically active surface. Therefore, the provided substrates are reacting to the target products, which are very important because of main aim of thermocatalytic reactor. In addition to experimental studies, the works focused on modeling of thermocatalytic process are becoming increasingly important. Besides the papers that describe in general the processes of chemical reactions [11,12], there are articles devoted to models of reactors and catalytic microreactors [2,3,13,14]. As it is shown in [13,15–22] for modeling mixture flows with a strong interaction of the surface and the liquid material, boundary conditions and appropriate closure in mathematical models are essential.

The main aim of this paper is to present a mathematical model of the flow of the mixture for compact thermocatalytic devices used for decomposition of hydrocarbons. Computational fluid dynamics (CFD) allows to model heat transfer,

chemical reaction and fluid flow processes in volume of devices. In Sections 2 and 3.1–3.8. we have showed the standard elements of CFD tools in volume (bulk). In Section 3.9, theoretical background to balance in the boundary layer has been presented. The main reaction which is considered at stoichiometric level has been discussed in 3.10. However, in standard code CFD the most important reaction , namely the methanol decomposition reaction over Ni_3Al, Eq. (114), is neglected. The user defined functions (UDF) adaptivity, presented in 4.2., covered the issues corresponding with proper catalytic reaction placement and proper reaction rates in specific conditions. Nevertheless, reaction rates are limited to the data provided in experiment which are sufficient in this particular case. Based on the example of mixture containing helium contaminated by methanol flowing in a horizontal microchannels heated to $500\,^{\circ}C$, the results of experiment were shown and compared with CFD calculations that have been expanded by UDFs. These extensions transformed the calculation mechanisms and algorithms of commercial codes adapting them for the microflows cases and increased chemical reactions rate on an interphase between fluid and solid. Results obtained on the way of numerical calculations were compared with experimental data receiving satisfactory compliance.

2 Basic definitions describing the mixture

The flow of a mixture of helium and methanol and methanol decomposition within catalytic chemical reaction, which creates the components: H_2, CO, CO_2, CH_4, H_2O, and at least one of the unknown compound, has been considered. Based on [11,23,24], the equations describing the mixture into several chemically reactive components, $m = 1, 2, \ldots,\ NS$, that may also be subject to a phase change, have been adopted. This could be the stream that is a component of exhaust gas (or a component of methanol decomposition reaction). For this reason, in the general formulation of gas dynamics mixtures, in addition to the basic unknown, which is a mass fraction of the component Y_m (mass of component / mass of mixture), there could occur a volume fraction of the component X_m specific for multiphase flows, where index m means component.

It was assumed that the continuum particle takes position $\overrightarrow{x}$ in time t, contains NS components, that arrived at $\overrightarrow{x}$ position during movement which started at $\overrightarrow{X}_m$ position, different for each component. Therefore the definition of the position for each continuum component is as follows:

$$\overrightarrow{x}_m = \overrightarrow{\chi}\left(\overrightarrow{X}_m, t\right), \qquad m = 1, 2, \ldots, NS, \tag{1}$$
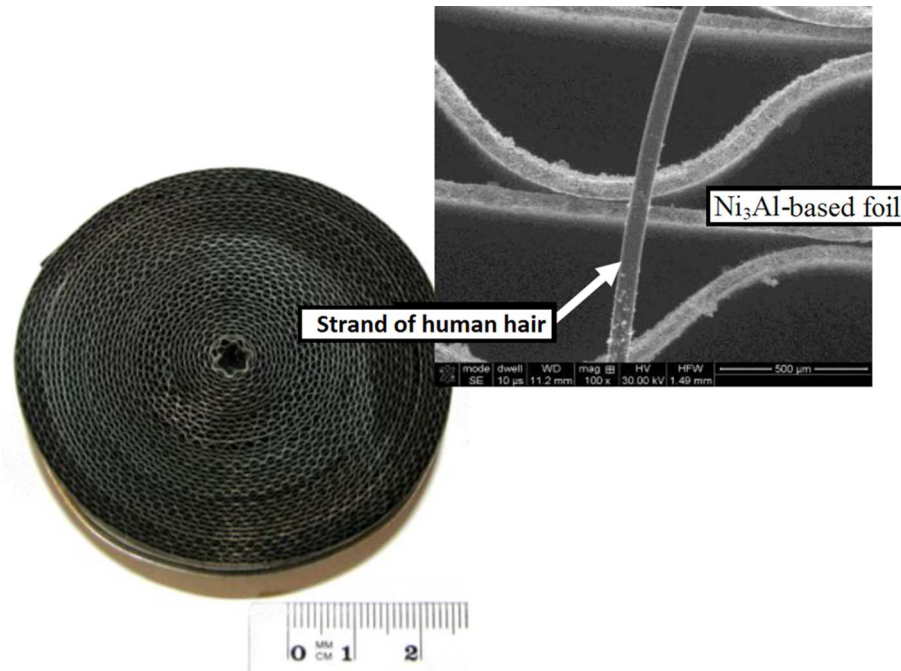
Figure 1: The example of one alloy foil packet based on intermetallic phase Ni$_3$Al rolled into a honeycomb and a comparison of film thickness Ni$_3$Al with the thickness of a human hair [1].

where NS is the number of components. This means that each component that penetrates through the $\overrightarrow{x}$ has its own velocity, described by the dependence

$$\overrightarrow{v}_m = \partial_t \; \overrightarrow{\chi}\left(\overrightarrow{X}_m, t\right) , \qquad m = 1, 2, \ldots, NS . \tag{2}$$

The density of the component, that is the component mass relative to the one of the volume unit of the mixture, is

$$\rho_m = \rho Y_m , \tag{3}$$

where Y_m is the mass fraction of the component divided by mass of the mixture, while ρ is the mixture density such as

$$\rho = \sum_{m=1}^{NS} \rho_m . \tag{4}$$

From Eqs. (3) and (4) appears that the sum of mass fractions equals one:

$$\sum_{m=1}^{NS} Y_m = 1 \ . \tag{5}$$

If X_m is the volume or mole fraction, the partial density is

$$\rho_m = \rho X_m \frac{W_m}{\overline{W}} \ , \tag{6}$$

where W_m is the molecular weight of mth component and $\overline{W}$ is average molecular weight, while X_m takes value from range of $0 \leq X_m \leq 1$, wherein for $X < 1$ the mixture is insatiable, and for $X = 1$ is saturated.

Since barycentric velocity of the mixture refers to the density of the mixture

$$\overrightarrow{v} = \frac{1}{\rho} \sum_m \rho \ \overrightarrow{v}_m \ , \qquad m = 1, 2, \ldots, NS \tag{7}$$

the diffusion velocity

$$\overrightarrow{V}_m = \overrightarrow{v} - \overrightarrow{v}_m \tag{8}$$

that summed for all components is to be zero:

$$\sum \rho_m \overrightarrow{V}_m = 0 \ . \tag{9}$$

3 Governing equations

The equation for the mass balance for each component is considered in stationary control volume thus that the fractions of the other ingredients are presented in the form of sources. Hence, a conservative form of this equation can be presented for $\rho_m = \rho Y_m$ as

$$\partial_t \left(\rho Y_m \right) + \mathrm{div} \left(\rho Y_m \overrightarrow{v}_m \right) = c_m^+ \tag{10}$$

or taking $\overrightarrow{V}_m = \overrightarrow{v} - \overrightarrow{v}_m$

$$\partial_t \left(\rho Y_m \right) + \mathrm{div} \left(\rho Y_m \overrightarrow{v} \right) = \mathrm{div} \left(\rho Y_m \overrightarrow{V}_m \right) + c_m^+ \ , \tag{11}$$

where c_m^+ is the rate of formation the mass component relative to a volume of the mixture. Thus, the formation of a component (or degradation) results from a chemical reaction.

The momentum balance equation is considered in a similar manner to the mass balance

$$\partial_t \left(\rho Y_m \vec{v}_m\right) + \text{div}\left(\rho Y_m \vec{v}_m \otimes \vec{v}_m\right) = \text{div}\ \overset{\leftrightarrow}{t}_m + \rho Y_m \vec{b}_m + \vec{m}_m^+\ , \qquad (12)$$

where $\otimes$ dyadic multiplicator, $\overset{\leftrightarrow}{t}_m = -p_m \overset{\leftrightarrow}{I} + \overset{\leftrightarrow}{\tau}_m$ is the Cauchy's momentum flux. In the case of gas mixture components $m = 1, 2, \ldots,\ NS$, it consists of a reversible pressure – p_m – or a viscous part $\overset{\leftrightarrow}{\tau}_m$ (dissipational). At a thermodynamic pressure p_m – unit tensor (Gibbs' idemfactor) $\overset{\leftrightarrow}{I}$ occurs. In turn, the mass force and source of momentum of a component are denoted by $\vec{b}_m$ and $\vec{m}_m^+$, respectively.

Next, we consider the balance of configuration forces

$$\partial_t \left(\rho Y_m f_m \dot{\chi}_m\right) + \text{div}\left(\rho Y_m f_m \dot{\chi}_m \vec{v}_m\right) = \text{div}\left(\vec{h}_m\right) + \rho Y_m(g_m + l_m) + \chi_m^+\ , \quad (13)$$

where f_m is (virtual) inertia of component, whose volume fraction expands (changes) with the rate, $(\dot{\chi}_m)$, $\vec{h}_m$ means a balanced flux χ_m, while g_m and l_m are external and internal driving force of phase transition. A source of configurational forces is designated as χ_m^+.

The balance of internal energy ϵ_m is defined as follows:

$$\partial_t \left(\rho_m \epsilon_m\right) + \text{div}\left(\rho_m \epsilon_m \vec{v}_m\right) = \text{div}\ \vec{q}_m + \text{tr}\left(\overset{\leftrightarrow T}{t}_m \overset{\leftrightarrow}{d}_m\right) + \vec{h}_m\ \text{grad}\left(\chi_m\right) +$$

$$\frac{1}{2}\rho_m f_m (\dot{\chi}_m)^2 -\ \rho_m g_m \chi_m +\ \rho_m r_m + e_m^+ \qquad (14)$$

where: $\vec{q}_m$ – heat flux, $\text{tr}\left(\overset{\leftrightarrow T}{t}_m \overset{\leftrightarrow}{l}_m\right)$ – mechanical power, $\frac{1}{2}\rho_m f_m (\dot{\chi}_m)^2$ – transformation power, $g_m \chi_m$ – power of the driving forces, $\rho_m r_m$ – radiation sources, e_m^+ – energy sources. It should be noted that the mechanical power takes into account the spatial gradients, $\overset{\leftrightarrow}{l}_m$

$$\overset{\leftrightarrow}{l}_m =\ \text{grad}\ \vec{v}_m = \vec{v}_m \otimes \nabla = \frac{\partial v_{i\ m}}{\partial x_j}\vec{e}_i \otimes \vec{e}_j = \overset{\leftrightarrow}{d}_m + \overset{\leftrightarrow}{\omega}_m\ , \qquad (15)$$

in which we distinguish a symmetrical rate of deformation of the component $\overset{\leftrightarrow}{d}_m = \overset{\leftrightarrow T}{d}_m$ and antisymmetric vorticity $\overset{\leftrightarrow T}{\omega}_m = -\overset{\leftrightarrow}{\omega}_m$. It should also take into account the balance of angular momentum

$$\overset{\leftrightarrow}{t}_m -\ \overset{\leftrightarrow T}{t}_m =\ \overset{\leftrightarrow +}{M}_m\ , \qquad (16)$$

where there is a source of angular momentum $\overset{\leftrightarrow}{M}{}^{+}_{m}$ (antisymmetric tensor).

In the balance of mixture, considered as a homogeneous continuum, these sources always cancel out entirely. Summing up the balance of each component and defining the following averages, we obtained respectively [11]:

$$\overset{\leftrightarrow}{t} = \sum_{m}^{NS} (\overset{\leftrightarrow}{t}_m + \rho_m \vec{v}_m \otimes \vec{v}_m) , \tag{17}$$

$$\vec{b} = \frac{1}{\rho} \sum \rho_m \vec{b}_m , \tag{18}$$

$$\vec{h} = \sum (\vec{h}_m - \rho_m f_m \dot{\chi}_m \vec{v}_m) , \tag{19}$$

$$g = \frac{1}{\rho} \sum \rho_m g_m , \tag{20}$$

$$l = \frac{1}{\rho} \sum \rho_m l_m , \tag{21}$$

$$f\dot{\chi} = \frac{1}{\rho} \sum \rho_m f_m \dot{\chi}_m , \tag{22}$$

$$v = \frac{1}{\rho} \sum \rho_m (v_m + \frac{1}{2}\vec{v}_m^2 + \frac{1}{2}f_m \dot{\chi}_m) - \frac{1}{2}\vec{v}^2 - \frac{1}{2}f\dot{\chi} , \tag{23}$$

$$\vec{q} = \Big[\sum \vec{q}_m - \overset{\leftrightarrow}{t}_m \vec{v}_m - \vec{h}_m (\chi_m - \chi) - $$
$$\rho_m f_m (\dot{\chi}_m - \dot{\chi}) \vec{v}_m + \rho_m (\epsilon_m + \frac{1}{2}\vec{v}_m^2 + \frac{1}{2}f_m \dot{\chi}_m) \vec{v}_m \Big] . \tag{24}$$

Then, we obtained the averages compounds for the mixture continuum, namely: firstly the mass balance:

$$\partial_t \rho + \operatorname{div}(\rho \vec{v}) = 0 , \tag{25}$$

secondly the balance of momentum for the continuum mixture defined as

$$\partial_t (\rho \vec{v}) + \operatorname{div}(\rho \vec{v} \otimes \vec{v}) = \operatorname{div}\left(\overset{\leftrightarrow}{t}\right) + \rho \vec{b} . \tag{26}$$

It should be mentioned that the momentum is related to the volume of the mixture, $\rho \vec{v}$, hence it expresses its integral dynamic characteristics.

The balance of internal energy takes the form

$$\partial_t (\rho \epsilon) + \operatorname{div}(\rho \epsilon \vec{v}) = \operatorname{div}\vec{q} + \operatorname{tr}\left(\overset{\leftrightarrow}{t}{}^T \overset{\leftrightarrow}{l}\right) + \vec{h} \cdot \operatorname{grad}\chi - \frac{1}{2}\rho f \dot{\chi}^2 + \rho r \tag{27}$$

while the balance of configuration power reduces to the expression

$$\partial_t \left(\rho f \dot{\chi} \right) + \text{div} \left(\rho f \dot{\chi} \overrightarrow{v} \right) = \text{div} \overrightarrow{h} + \rho(g+l) \,. \tag{28}$$

The balance of angular momentum satisfies the condition

$$\overleftrightarrow{t} = \overleftrightarrow{t}^T \,, \tag{29}$$

The total flux of momentum meets the balance of angular momentum It is worth mentioning that the total momentum flux of the mixture is expressed as

$$\overleftrightarrow{t} = -p \overleftrightarrow{I} + \overleftrightarrow{\tau} + \overleftrightarrow{r} + \overleftrightarrow{\tau}^{dyf} + \overleftrightarrow{\tau}^{rad} + \overleftrightarrow{\tau}^{trans} = -p \overleftrightarrow{I} + \overleftrightarrow{\tau}^c \,, \tag{30}$$

where in addition to a reversible component, namely the thermodynamic pressure, p; there are dissipational ingredients: $\overleftrightarrow{\tau}$ – the flux of viscous stress, $\overleftrightarrow{r}$ – Reynolds' turbulent flux, $\overleftrightarrow{\tau}^{dyf}$ – momentum flux resulting from the diffusion, $\overleftrightarrow{\tau}^{rad}$ – momentum flux resulting from the radiation, and $\overleftrightarrow{\tau}^{trans}$ – momentum flux resulting from the transpiration. For these balances the internal sources are self-sustainable, i.e.,

$$\sum c_m^+ = \sum W_m \dot{\omega}_m = 0 \,, \qquad m = 1, 2, \ldots, NS \,, \tag{31}$$

where W_m is a molecular mass of a component, $\dot{\omega}_m$ is the molar rate (in moles of substance per cubic meter per second. Similar situation is realized for other sources, as following

$$\sum (\overrightarrow{m}_m^+ + c_m^+ \overrightarrow{v}_m) = 0 \,, \tag{32}$$

$$\sum \left(\overleftrightarrow{M}_m^+ \right) = 0 \,, \tag{33}$$

$$\sum \left(\chi_m^+ + c_m^+ f_m \dot{\chi}_m \right) = 0 \,, \tag{34}$$

$$\sum \left[e_m^+ + \overrightarrow{m}_m^+ \cdot \overrightarrow{v}_m + \chi_m^+ \chi_m + c_m^+ \left(\epsilon_m + \frac{1}{2} \overrightarrow{v}_m^2 + \frac{1}{2} f_m \dot{\chi}_m \right) = 0 \right] \,. \tag{35}$$

In the case of saturated mixture $\dot{\chi} = 0$ all of the above equations greatly simplify and have classic single-phase form. It is also worth to mention that the parameter of inertia, f, is some kind of measure for the surface rate of the interface in a mixture [25–27].

3.1 Pressure of the mixture and classical equation of state

Thermal equation of mixture state which components are gases satisfying the ideal gas equation with the same temperature T, has also a form of the ideal gas law,

$$p = \rho R T , \tag{36}$$

where pressure, p, density, ρ, and the gas constant, R, are some of the sums for all the components contained in the considered point. The gas constant is defined as

$$R = \frac{R_u}{W} , \tag{37}$$

where $R_u = 8314.46$ J/(kmol K) is the universal gas constant, while W is a molecular weight of mixture. The individual components of pressure are given by the formula:

$$p_m = \rho Y_m R_m T , \tag{38}$$

where individual gas constant R_m for each component is calculated similarly to Eq. (37), namely

$$R_m = \frac{R_u}{W_m} , \tag{39}$$

where W_m is the molecular weight of the m-th component.

We know from the Dalton law of ideal gases for the mixture that

$$p = \sum_{m=1}^{NS} p_m = \sum_{m=1}^{NS} \rho Y_m R_m T = \rho \left(\sum_{m=1}^{NS} Y_m R_m \right) T = \rho R T , \tag{40}$$

where the gas constant of the mixture is calculated according to the formula

$$R = \sum_{m=1}^{NS} Y_m R_m . \tag{41}$$

We can notice that in the case of using variables straights in the numerics $\mathcal{Q} = \{\rho, \ \vec{v}, \ p, \ Y_m\}$ and the mixture pressure becomes basic unknown in the system.

3.2 Elastic constant of the mixture

In caloric perfect gas, which is a mixture of ideal gases, isentropic exponent takes the form

$$\kappa = \frac{c_p}{c_v} = \frac{C_p}{C_v} . \tag{42}$$

The ratio of specific heat capacities of the mixture is also constant, where c_p and c_v are related to substance per kilogram, and C_p and C_v to the mole substance. For ideal gas c_p and c_v also designate a second elastic constant, which is the individual gas constant

$$R = c_p - c_v \ . \tag{43}$$

In analogy to Eq. (41), the dependence on the specific heat capacity is defined at constant pressure, c_p, while the specific heat capacity is defined at constant volume, c_v:

$$c_p = \sum_{m=1}^{NS} Y_m c_{p(m)} \quad , \qquad c_v = \sum_{m=1}^{NS} Y_m c_{v(m)} \ , \tag{44}$$

where $c_{p(m)}$, $c_{v(m)}$ are the specific heat capacity at constant pressure and specific heat capacity at constant volume for components $m = 1, 2, \ldots, NS$ of gas mixture, respectively. On the other hand, substituting from Eqs. (43) and (37) to Eq. (42) we attain

$$\kappa = \frac{c_p}{c_p - \frac{R_u}{W}}. \tag{45}$$

Specific molar heat capacities of each component $C_{p(m)}^0$ at pressure of 1 atm can be calculated using the formula

$$\frac{C_{p(m)}^0}{R} = \sum_{n=1}^{NS} a_{n(m)} T^{(n-1)} \ , \quad n = 1, 2, 3, 4, 5 \ , \tag{46}$$

where constants $a_{n(m)}$ are tabulated in procedures of commercial codes [11,28] or in the works of the classics [29–31]. There are ratios between specific heat capacities of each mixture components ($c_{p(m)}$ and $c_{v(m)}$) per kilogram of substance and ($C_{p(m)}$ and $C_{v(m)}$) per mole of substance:

$$c_{p(m)} = \frac{C_{p(m)}}{W_m} \ , \tag{47}$$

$$c_{v(m)} = \frac{C_{v(m)}}{W_m} \ . \tag{48}$$

In turn, as the specific heat capacities of the entire mixture can be expressed in sequences

$$C_p = \sum_{m=1}^{NS} C_{p(m)} X_m \ , \tag{49}$$

$$c_p = \sum_{m=1}^{NS} c_{p(m)} Y_m = \frac{C_p}{W} \ , \tag{50}$$

$$C_v = \sum_{m=1}^{NS} C_{v(m)} X_m \ , \tag{51}$$

$$c_v = \sum_{m=1}^{NS} c_{v(m)} Y_m = \frac{C_v}{W} \ . \tag{52}$$

The values of the specific heat capacities are essential to determine the internal energy and enthalpy of the gas mixture which has a direct contribution to the energy balance.

3.3 Internal energy and viscous stress tensor of mixture

Specific internal energy, related to the unit mass of the component equals

$$\epsilon = \sum_{m=1}^{NS} \epsilon_m Y_m = \frac{\overline{\epsilon}}{W} \ , \tag{53}$$

where ϵ_m, in the easiest possible way, is defined as a function of temperature-dependent $\epsilon_m(T)$:

$$\epsilon_m(T) = \epsilon_m^{form} + c_{v(m)} T \ , \tag{54}$$

where ϵ_m^{form} is the energy of formation at a reference temperature. Additionally, ϵ could be related to one mole $\overline{\epsilon}$ and then

$$\epsilon = \sum_{m=1}^{NS} \overline{\epsilon}_m X_m \ . \tag{55}$$

Assuming that all components of the mixture have the same velocity, $\overrightarrow{v}$, and the same gradients, it is expected that the expression for the tensor of mixture viscous stress is a classic Stokes formula

$$\overset{\leftrightarrow}{\tau} = 2\mu \left[\overset{\leftrightarrow}{d} - \frac{1}{3} \text{div} \left(\overrightarrow{v} \right) \overset{\leftrightarrow}{I} \right] + \mu' \text{div} \left(\overrightarrow{v} \right) \overset{\leftrightarrow}{I} \ , \tag{56}$$

where rate of deformation is

$$\overset{\leftrightarrow}{d} = \frac{1}{2} \left(\nabla \otimes \overrightarrow{v} + \overrightarrow{v} \otimes \nabla \right) = \frac{1}{2} \left(\frac{\partial v_i}{\partial x_j} + \frac{\partial v_j}{\partial x_i} \right) \overrightarrow{e}_i \otimes \overrightarrow{e}_j = d_{ij} \overrightarrow{e}_i \otimes \overrightarrow{e}_j = \overset{\leftrightarrow}{d}{}^T \ , \tag{57}$$

where $\overset{\leftrightarrow}{d}{}^{T}$ is the transposition of the rate of deformation while μ is the dynamic viscosity of the mixture, μ' is the coefficient of second viscosity of the mixture, typically equals zero, that is widely described in [32,33]. Then it was assumed that the stresses in the viscous mixture is the sum of the viscous stress of the individual components

$$\overset{\leftrightarrow}{\tau} = \sum_{m}^{NS} \overset{\leftrightarrow}{\tau}_{m} \; . \tag{58}$$

This brought the formula for the viscosity of the mixture called Wilke formula [34]:

$$\mu = \sum_{m=1}^{NS} \frac{X_m \mu_m}{\sum_{m'=1}^{NS} X_m X_{m'} \Phi_{mm'}} = \sum_{m=1}^{NS} \frac{Y_m \mu_m}{W_m \left(\sum_{m'=1}^{NS} \frac{Y_{m'} \Phi_{mm'}}{W_m} \right)} \; , \tag{59}$$

where $\mu_m = \mu_m(T)$ is the viscosity of the component, X_m is the molar fraction of a component m in the mixture, while $\Phi_{mm'}$ is the Wilke matrix taking into account mm' interaction of mixture components, where $m \neq m'$ [34].

3.4 Balance of total mixture energy

Balance equation of the total energy (internal + kinetic) in a homogeneous mixture model consists of

- a temporal change of balanced quantity,
- fluxes of this quantity that leave or infiltrate the control area,
- the source parts.

Balance of the total mixture energy is presented as follows [11,24,35]:

$$\partial_t \left(\rho e \right) + \; \mathrm{div}(\rho e \overrightarrow{v}) = \mathrm{div} \left(\overrightarrow{q} + \; \overrightarrow{q}^{\,t} + \overset{\leftrightarrow}{t} \; \overrightarrow{v} + \overrightarrow{q}^{\,D} + \overrightarrow{q}^{\,rad} \right) +$$

$$\rho r + \rho \overrightarrow{b} \cdot \overrightarrow{v} + \sum_{m=1}^{NS} \rho h_m W_m \dot{\omega}_m \; , \tag{60}$$

where $e = \epsilon + \overrightarrow{v}^{\,2}/2$ is the sum of internal and kinetic energy, $\overrightarrow{q}$ and $\overrightarrow{q}^{\,t}$ are the molecular and turbulent heat fluxes, respectively, $\overset{\leftrightarrow}{t} \; \overrightarrow{v}$ is the mechanical energy flux, $\overrightarrow{q}^{\,D}$, $\overrightarrow{q}^{\,rad}$ are the diffusion and the radiative heat flux of the mixture, $\dot{\omega}_m$ is is chemical production rate of the mth species and

$$h_m = \epsilon_m + \frac{p_m}{\rho_m} \tag{61}$$

is the enthalpy component relative to mass unit of the component.

Total momentum flux $\overset{\leftrightarrow}{t} = -p\,\overset{\leftrightarrow}{I} + \overset{\leftrightarrow c}{\tau}$ is divided into elastic reversible part ($p\,\overset{\leftrightarrow}{I}$, first order derivatives) and mechanical diffusion part $\overset{\leftrightarrow c}{\tau}$. Then, the part with mechanical reversible flux of momentum $-p\,\overset{\leftrightarrow}{I}\,\overrightarrow{\upsilon} = -p\,\overrightarrow{\upsilon}$ moves to the left to give

$$\partial_t\,(\rho e) + \ \mathrm{div}\left[\left(e + \frac{p}{\rho}\right)\rho\,\overrightarrow{\upsilon}\right] =$$
$$\mathrm{div}\left(\overrightarrow{q} + \ \overrightarrow{q}^{\,t} + \overset{\leftrightarrow c}{\tau}\,\overrightarrow{\upsilon} + \overrightarrow{q}^{\,D} + \overrightarrow{q}^{\,h} + \overrightarrow{q}^{\,rad}\right) + S_e \ , \tag{62}$$

where S_e is the energy source in W/m^3. In the case of enthalpy formulation, should be used the following dependence

$$\rho e = \rho h + \rho\frac{\overrightarrow{\upsilon}^2}{2} - p \ . \tag{63}$$

In the literature is also described the total enthalpy

$$h^c = h + \ \frac{\overrightarrow{\upsilon}^2}{2} \ . \tag{64}$$

A detailed description of the individual components of the energy fluxes is presented in the next paragraph.

Bearing in mind that the energy and enthalpy refer to mass unit of each component, the enthalpy and internal energy of the mixture are determined using mass fractions Y_m [36]

$$h = \epsilon + \frac{p}{\rho} = \sum_{m=1}^{NS} Y_m \epsilon_m + \frac{1}{\rho}\sum_{m=1}^{NS} p_m = \sum_{m=1}^{NS} Y_m\left(\epsilon_m + \frac{p_m}{\rho Y_m}\right) = \sum_{m=1}^{NS} Y_m h_m \ . \tag{65}$$

Treating each component as a thermally perfect gas, we attain specific enthalpy, which is a function of temperature

$$h_m\,(T) = h_m^{form} + \int_{T_0}^{T} c_{p(m)}\,(T')\,dT' \ , \tag{66}$$

where h_m^{form} is the heat of 'forming' the component in temperature $T_0 = (273 + 25)$ K, while $c_{p(m)}$ is specific heat capacity at constant pressure. Caloric equation for perfect gas, where specific heat capacity, c_p, does not depend on temperature, comes from Eq. (66), which is simplified into the well-known formula

$$h_m\,(T) = h_m^{form} + c_{p(m)}T \ . \tag{67}$$

Thus, combining (65) and (66) yields

$$h = \sum_{m=1}^{NS} Y_m h_m^{form} + \int_{T_0}^{T} \sum_{m=1}^{NS} Y_m c_{p(m)} \left(T'\right) dT' = \sum_{m=1}^{NS} Y_m h_m^{form} + \int_{T_0}^{T} c_p \left(T'\right) dT' \,,$$

(68)

where c_p is the total specific heat capacity of the mixture at constant pressure. It leads to

$$h = \sum_{m=1}^{NS} Y_m h_m^{form} + c_p T$$

(69)

for mixture of calorie perfect gas.

3.5 Energy fluxes

It was assumed that the molecular thermal conductivity of the mixture is determined by one coefficient λ, which is a sum of contributions from the conductivity of each components λ_m, $m = 1, \ldots, NS$. In the case of the molecular heat flux, we remain of the simplest version of the Fourier heat conduction

$$\overrightarrow{q} = \lambda \nabla T \,,$$

(70)

although in the flame zone, where isotropy expressed in Eq. (70) seems to be compromised, it would be more reasonable to introduce another conductivity in normal direction to the flame, $\lambda_\perp$, and in other tangential direction, $\lambda_\parallel$, therefore

$$\overrightarrow{q} = \left[\lambda_\perp \overrightarrow{n} \otimes \overrightarrow{n} + \lambda_\parallel \left(\overset{\leftrightarrow}{I} - \overrightarrow{n} \otimes \overrightarrow{n} \right) \nabla T \right] \,.$$

(71)

where: $\lambda_\perp \overrightarrow{n} \otimes \overrightarrow{n} + \lambda_\parallel \left(\overset{\leftrightarrow}{I} - \overrightarrow{n} \otimes \overrightarrow{n} \right)$ is responsible for heat transfer within the layer, therefore, it has tangential component $\left(\overset{\leftrightarrow}{I} - \overrightarrow{n} \otimes \overrightarrow{n} \right)$ and normal component $(\overrightarrow{n} \otimes \overrightarrow{n})$ of surface conductivity, while $\left(\overset{\leftrightarrow}{I} - \overrightarrow{n} \otimes \overrightarrow{n} \right)$ defines the surface Gibbs identity. The thermal conductivity of a single component usually depends on the temperature, T, therefore $\lambda_m = \lambda_{(m)}(T)$. It should be added that in accordance with the work [37], the averaging of conductivity for whole mixture is conducted by molar fraction X_m from Eq. (6), not by mass fraction Y_m. Hence $\lambda \left(\lambda_{(m)}, X_m \right)$ could be defined as

$$\lambda = \frac{1}{2} \left(\sum_{m=1}^{NS} X_m \lambda_{(m)} + \frac{1}{\sum_{m=1}^{NS} \frac{X_m}{\lambda_{(m)}}} \right) \,.$$

(72)

Using the atomic weight of the mixture, W, we transform (72) to

$$\lambda = \frac{1}{2} \left(W \sum_{m=1}^{NS} \frac{Y_m \lambda_{(m)}}{W_m} + \frac{1}{W \sum_{m=1}^{NS} \frac{Y_m}{W_m \lambda_{(m)}}} \right) . \tag{73}$$

Following by Umov and Volter, we define mechanical energy flux, $\overset{\leftrightarrow}{t} \vec{v}$, as the product of the total mixture flux of momentum (reversible + irreversible) from Eq. (30) and the barycentric velocity of the mixture from Eq. (7):

$$\vec{q}^m = \overset{\leftrightarrow}{t} \vec{v} = \left(-p \overset{\leftrightarrow}{I} + \overset{\leftrightarrow}{\tau} + \overset{\leftrightarrow}{r} + \overset{\leftrightarrow}{\tau}^{dyf} + \overset{\leftrightarrow}{\tau}^{rad} + \overset{\leftrightarrow}{\tau}^{trans} \right) \vec{v} = -p \overset{\leftrightarrow}{I} \vec{v} + \overset{\leftrightarrow}{\tau}^c \vec{v} . \tag{74}$$

In the literature, the description of $\vec{q}^m$ is usually limited to the reversible part with thermodynamic pressure, p, and to one dissipation part, mainly the stress viscous mixture flux, $\overset{\leftrightarrow}{\tau}$ [38].

In turn, turbulent heat flux, $\vec{q}^t$, is the one, which is not easy phenomenologically shut, and even harder to verify by measurement [15,39]. The most common solution adopted by renowned research centers, is a classic method of turbulent transport of heat assigned the same drive mechanisms, which describe the turbulent transport of momentum

$$\vec{q}^t = \lambda_t \nabla T = \frac{c_p \mu_t}{\mathrm{Pr}_t} \nabla T , \tag{75}$$

where $\lambda_t = c_{pt}/\mathrm{Pr}_t$ – turbulent conductivity determined by c_p, μ_t, and Pr_t which are the specific heat capacity, turbulent viscosity of the mixture, and the turbulent Prandtl number, respectively.

Duffors heat flux occurs in a strong gradient of component concentration and is designated as [40]

$$\vec{q}^D = R_u T \sum_{m=1}^{NS} \sum_{m'}^{NS} \left(\frac{X_m \alpha_{m'}}{W_m D_{mm'}} \right) \left(\vec{V}_m - \vec{V}_{m'} \right) , \tag{76}$$

where, $\alpha_{m'}$ – thermal diffusion coefficient, $D_{mm'}$ – binary diffusivity between components (m) and (m').

Radiative heat flux is defined in the implicit form of the integro-differential equations

$$\mathrm{div} \, \vec{q}^{rad} = \alpha \left[4e_b - g \right] , \tag{77}$$

where α is the absorption coefficient, e_b is the transmit power of the black body, g is the specific energy of radiation.

The heat flux of binary diffusivity is a function of the diffusion velocities and enthalpies being lifted by them

$$\overrightarrow{q}^h = \rho \sum_{m=1}^{NS} h_m Y_m \overrightarrow{V}_m \, , \tag{78}$$

where $\overrightarrow{V}_m$ is the diffusivity velocity of the component (m) and h_m is enthalpy. This part is usually omitted.

3.6   Diffusion-kinetic equation

Diffusion-kinetic equation for mass fraction Y_m of each $NS-1$ mixture component can be put in conservative form [11,41]:

$$\partial_t \left(\rho Y_m \right) + \mathrm{div} \left(\rho Y_m \overrightarrow{v} \right) = -\mathrm{div} \left(\overrightarrow{J}_m + \overrightarrow{J}_m^t \right) + \dot{\omega}_m W_m \, , \qquad m = 1 \, , \ldots , NS - 1 \, , \tag{79}$$

where ρ and $\overrightarrow{v}$ are the density and the average velocity of the mixture, respectively, Y_m is the mass fraction of mth component taking part in the reaction, $\overrightarrow{J}_m$ is the diffusion flux of mth diffusible component relative to the average velocity $\overrightarrow{v}$, while $\overrightarrow{J}_m^t$ is the turbulent diffusion flux. Knowing the fractions Y_m each of the $NS-1$ component, the mass fraction of the last component can be calculated from the condition that the sum of the mass fractions is equal to unity:

$$Y_{NS} = 1 - \sum_{m=1}^{NS-1} Y_m \, . \tag{80}$$

Additionally, the averaged turbulent production of component describes the source of chemical production of mth component $\dot{\omega}_m$ multiplied by the molecular weight of mth component W_m. If turbulent diffusive flux $\overrightarrow{J}_m^t$ is omitted in the model, the production $\dot{\omega}_m$ only describes the molecular source.

Mass fraction Y_m is the primary conservative variable, whose evolution of the equation is formulated for. However, sometimes the molar fraction X_m is more convenient to express the boundary conditions and the source term. Transition between Y_m and X_m is as follows:

$$Y_m = \frac{W_m}{\overline{W}} X_m, \quad X_m = \frac{Y_m \overline{W}}{W_m} \, . \tag{81}$$

The average molecular weight $\overline{W}$ could be defined in three ways:

$$\overline{W} = \left(\sum_{m=1}^{NS} \frac{Y_m}{W_m} \right)^{-1} , \tag{82}$$

$$\overline{W} = \sum_{m=1}^{NS} X_m W_m , \tag{83}$$

$$\overline{W} = \frac{\sum_{m=1}^{NS} [X_m] W_m}{\sum_{m=1}^{NS} [X_m]} , \tag{84}$$

where $[X_m]$ means the molar concentration

$$[X_m] = X_m \frac{\rho}{\overline{W}} . \tag{85}$$

In general, diffusion fluxes, $\overrightarrow{J}_m$, depend on the diffusion velocity, $\overrightarrow{V}_m$, in the following way:

$$\overrightarrow{J}_m = \rho Y_m \overrightarrow{V}_m . \tag{86}$$

The best proven closure on $\overrightarrow{V}_m$ is Dixon-Lewis' formula [42]

$$\overrightarrow{V}_m = \frac{1}{X_m \overline{W}} \sum_{m' \neq m}^{NS} W_{m'} D_{mm'} \, \overrightarrow{d}_{m'} - \frac{D_m^T}{\rho Y_m} \frac{\nabla T}{T} , \tag{87}$$

where $D_{mm'}$ and D_m^T are the coefficients of multicomponents and temperature diffusion, respectively, while $\overrightarrow{d}_m$ is the diffusion vector

$$\overrightarrow{d}_m = \nabla X_m + (X_m - Y_m) \frac{\nabla p}{p} + \frac{\rho}{p} \sum_{m'}^{NS} Y_m Y_{m'} (\overrightarrow{g}_{m'} - \overrightarrow{g}_m) , \tag{88}$$

where the last parameter containing mass forces $\overrightarrow{g}_m$, which disappeared after free transport of gas, and p is the thermodynamic pressure of the mixture. Following part: $(X_m - Y_m) \nabla p / p$ means that the pressure gradient may cause the diffusion strength separating the components of different molecular weights. However, except for isotope separation of gas, the member is usually negligible [42]. Generally, the formula for diffusion velocity (87) influence on the sum of all diffusion fluxes, $\overrightarrow{J}_m$, which does not equal zero. However, equal to zero can be the following formula:

$$\overrightarrow{V}_m = -\frac{D_{(m)}}{X_m} \overrightarrow{d}_m - \frac{D_m^T}{\rho Y_m} \frac{\nabla T}{T} . \tag{89}$$

Using mass fractions Y_m we obtained the Dixon-Lewis expression

$$\overrightarrow{J}_m = \rho Y_m \overrightarrow{V}_m = -\rho \hat{D}_m \nabla Y_m - D_m^T \frac{\nabla T}{T} \, , \qquad (90)$$

where diffusion coefficient $\hat{D}_m$ has a form

$$\hat{D}_m = \left[\frac{-1}{\nabla Y_m \cdot \nabla Y_m} \right] \frac{W_m}{\overline{W}^2} \sum_{m \neq m'}^{NS} W_{m'} D_{mm'} \nabla X_{m'} \nabla Y_m \qquad (91)$$

or entering coefficient $D_{(m)}$ from (89) can be attained

$$\hat{D}_m = D_{(m)} \frac{W_m}{\overline{W}} \left[\frac{\nabla X_m \, \nabla Y_m}{\nabla Y_m \, \nabla Y_m} \right] \, . \qquad (92)$$

3.7   The rate of chemical reaction

We assume that the decomposition process (or combustion process and other chemical processes) is determined by the elementary chemical reactions $(\alpha) = 1, \ldots, I$, between mth components. All of the elementary reactions are standard for gases

$$\sum_{m=1}^{NS} \nu'_{m(\alpha)} \chi_m \Longleftrightarrow \sum_{m=1}^{NS} \nu''_{m(\alpha)} \chi_m \, , \qquad (\alpha) = 1, \ldots, I \, , \qquad (93)$$
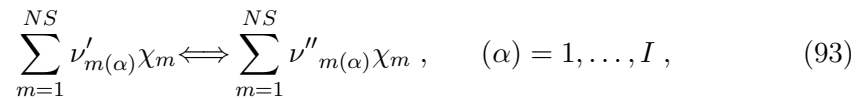
where NS is the amount of chemical components designated by χ_m and I is the number of the elementary chemical reactions. The stoichiometric matrix coefficients $\nu_{m(\alpha)}$ are integers: $\nu'_{m(\alpha)}$ is the coefficient of mth component for the progressive αth reaction of nonpositive value, while $\nu''_{m(\alpha)}$ is the stoichiometric coefficient for the reverse reaction of the nonnegative value. Elementary reactions usually contain only three or four components, hence the matrices $\nu_{m(\alpha)}$ are 'rare' for most of the reaction.

The rate of production of the component $\dot{\omega}_m$ depends on all reactions occurring at the time, and hence is equal to

$$\dot{\omega}_m = \sum_{(\alpha)=1}^{I} \nu_{m(\alpha)} q_{(\alpha)} \, , \qquad (94)$$

where total stoichiometric coefficient equals $\nu_{m(\alpha)} = \nu''_{m(\alpha)} + \nu'_{m(\alpha)}$, while $q_{(\alpha)}$ is the αth chemical reaction rate, defined by the following general formula of

chemical reactions [11,40,41]

$$q_{(\alpha)} = k^t_{(\alpha)} \prod_{m=1}^{NS} [X_m]^{\left|\nu'_{m(\alpha)}\right|} - k^r_{(\alpha)} \prod_{m=1}^{NS} [X_m]^{\left|\nu''_{m(\alpha)}\right|} , \tag{95}$$

where $[X_m]$ is the molar concentration of mth component and $k^t_{(\alpha)}$, $k^r_{(\alpha)}$ are constants of transition in progress and reversing of the chemical reaction, respectively. Progress factor for (α)th reaction has the Arrhenius form [40,41]

$$k^f_{(\alpha)} = A_{(\alpha)} T^{\beta\,(\alpha)} \exp\left(\frac{-E_{(\alpha)}}{R_u T}\right), \qquad f = t,r , \tag{96}$$

where: $A_{(\alpha)}$ – dimensionless factor, $\beta_{(\alpha)}$ – exponent of temperature, $E_{(\alpha)}$ – activation energy are essential data to specify the chemical reactions. The constants of reversing of the chemical reaction $k^r_{(\alpha)}$ are combined with the constants of transition in progress of the chemical reaction $k^t_{(\alpha)}$ by the equilibrium constant for (α)th reaction $K^C_{(\alpha)}$

$$k^r_{(\alpha)} = \frac{k^t_{(\alpha)}}{K^C_{(\alpha)}} , \tag{97}$$

which can be founded by closure [11]

$$K^C_{(\alpha)} = K_{p(\alpha)} \left(\frac{p_{atm}}{RT}\right)^{\sum_{m=1}^{NS} \nu_{m(\alpha)}} , \tag{98}$$

where $p_{atm} = 1$ atm and the equilibrium constant $K_{p(\alpha)}$ equals

$$K_{p(\alpha)} = \exp\left(\frac{\Delta S^0_{(\alpha)}}{R} - \frac{\Delta H^0_{(?\alpha)}}{RT}\right) . \tag{99}$$

The symbol Δ refers to the change that occurs in the full transition between the components αth the reaction and its product. In particular, the changes of entropy, $\Delta S^0_{(\alpha)}$, and enthalpy, $\Delta H^0_{(\alpha)}$, are calculated as

$$\frac{\Delta S^0_{(\alpha)}}{R} = \sum_{m=1}^{NS} \nu_{m(\alpha)} \frac{S^0_m}{R} , \tag{100}$$

$$\frac{\Delta H^0_{(\alpha)}}{RT} = \sum_{m=1}^{NS} \nu_{m(\alpha)} \frac{H^0_m}{RT} . \tag{101}$$

3.8 The reactions with a catalyst

In certain types of reactions, the presence of 'third body' is required for the process to occur – as happens in the case of dissociation or recombination, as explained on the example

$$\text{H}+\text{O}_2+\text{M} \Longleftrightarrow \text{HO}_2+\text{M} \; . \tag{102}$$

In the processes taking place with the presence of 'third body', the rate of reaction $q_{(\alpha)}$, determined earlier in formula (95), must explicitly depend on the mass participation of 'third body' by factor $\alpha_{m(\alpha)}$ [37]

$$q_{(\alpha)} = \left(\sum_{m=1}^{NS} \alpha_{m(\alpha)} \left[X_m \right] \right) \left(k_{(\alpha)}^f \prod_{m=1}^{NS} \left[X_m \right]^{\left| \nu'_{m(\alpha)} \right|} - k_{(\alpha)}^r \prod_{m=1}^{NS} \left[X_m \right]^{\left| \nu''_{m(\alpha)} \right|} \right) \; . \tag{103}$$

If all components of the mixture play the same and equal role of 'third body', then $\alpha_{m(\alpha)} \equiv 1$ and the first coefficient, Eq. (103), is the total concentration of the mixture:

$$[M] = \sum_{m=1}^{NS} [X_m] \equiv \frac{p}{RT} \; . \tag{104}$$

If, as is often the case, some of the components operate as 'third body' more effectively than others, the factors $\alpha_{m(\alpha)}$ must take it into account. On the contrary, for a component that does not exist in a 'third body' $\alpha_{m(\alpha)} \equiv 0$.

From numerical point of view, division into producing and destructive units is convenient

$$\dot{\omega}_m = \dot{C}_m - \dot{D}_m \; , \tag{105}$$

where in accordance with [43]:

$$\dot{C}_m = \sum_{\alpha=1}^{I} \nu'_{m(\alpha)} k_{(\alpha)}^r \prod_{m'=1}^{NS} \left[X_{m'} \right]^{\nu''_{m'\alpha}} + \sum_{\alpha=1}^{I} \nu''_{m(\alpha)} k_{(\alpha)}^f \prod_{m'=1}^{NS} \left[X_{m'} \right]^{\nu'_{m'\alpha}} \; , \tag{106}$$

$$\dot{D}_m = \sum_{\alpha=1}^{I} \nu'_{m(\alpha)} k_{(\alpha)}^f \prod_{m'=1}^{NS} \left[X_{m'} \right]^{\nu''_{m'\alpha}} + \sum_{\alpha=1}^{I} \nu''_{m(\alpha)} k_{(\alpha)}^r \prod_{m'=1}^{NS} \left[X_{m'} \right]^{\nu'_{m'\alpha}} \; . \tag{107}$$

When the 'third body' takes part in the reaction, the parameters $\dot{C}_m$ and $\dot{D}_m$ should be multiplied by the concentration

$$[M] = \sum_{m=1}^{NS} \alpha_{m(\alpha)} [X_m] \; . \tag{108}$$

In the specific case, assuming that the rate of change is only the result of mass flow rate coming from the surface reaction, a useful form for the component destruction part formula is the time of relaxation τ_m, i.e,

$$\dot{\omega}_m = \dot{e}_m - \frac{[X_m]}{\tau_m} \, , \tag{109}$$

where the time of relaxation is expressed as

$$\tau_m = \frac{[X_m]}{\dot{D}_m + \epsilon} \, , \tag{110}$$

where $\epsilon \sim 10^{-50}$ is constant to prevent the situation, in which $[X_m]$ and $\dot{D}_m$ at the same time come together to be zero.

3.9 Balance in the boundary layer

Numerous problems of gas-dynamic boundary layer increase as a result of composition with the chemical phenomena that are taking place in the vicinity of solids. Flow model of chemical reactions, discussed in Subsection 3.7, refers to both mechanical, thermal and chemical issues of the phenomena occurring in volume (bulk). Phenomena occurring on the surface of the combustion chamber is characterized by the complete anisotropy. Apart from the volume production of component $\dot{\omega}_m$, the reaction of the surface absorption also described chemical kinetics, and therefore they should be treated as some surface source (or discounts) for the ingredients Y_m [44].

Chemical vapour deposition describes the chemical phenomena of the spraying the single-crystal films that change the electrical and optical properties of the surface. The main task is to model the heterogeneous surface reactions catalysed by surfaces.

The deposition of films of heterogeneous reactant is also associated with the process of heat transfer through the wall. For low wall temperature, the heterogeneous reaction rate is low. In conditions of low pressure and low flow speed, more important become the effects associated with heat exchange and mass transfer, such as natural convection, buoyancy, the effects of acceleration, which can cause complex patterns of transport in the layer. A similar influence can occurr for rarefied gas, hence these parameters should be included in the closure of determining the source or vent $\dot{\omega}_m$. Balance equation of components, in the channel surface oriented by normal vector $\overrightarrow{n}$ has the following condition for the flux $\overrightarrow{J}_m$:

$$\left[\rho \overrightarrow{v} Y_m + \overrightarrow{J}_m \right] \overrightarrow{n} = \dot{\omega}_m^n \, , \tag{111}$$

where $\overrightarrow{v}$ – velocity of the mixture, $v_n = \overrightarrow{v} \cdot \overrightarrow{n}$ – normal component of velocity to the inlet wall, Y_m – mass fraction of the mth component, $\overrightarrow{J}_m$ – diffusion flux of the mth component, $\dot{\omega}_m^n$ – deposition rate of the mth component.

Since the components may leave or enter the area at different velocities, the normal component of the mixture velocity must be [11]

$$\rho v_n = \sum_{m=1}^{n_{gas}} \dot{\omega}_m^n = - \sum_{m=1}^{n_{surf}} \dot{\omega}_m^n \,, \tag{112}$$

where n_{gas} and n_{surf} are the number of gas components and the number of surface phase components, respectively. The rate of surface production $\dot{\omega}_\alpha^n$ is usually based on the Arrhenius equation [12], and can be extended as follows:

$$\dot{\omega}_{m,(\alpha)}^n = \nu_{m,\ (\alpha)} W_m T^{\beta(\alpha)} A_{(\alpha)} \prod_{m'reaktans} C_{m'}^{\hat{\nu}_{m',(\alpha)}} \exp\left(\frac{E_{(\alpha)}}{RT}\right) \,, \tag{113}$$

where: $\nu_{m,\ (\alpha)}$ – molar stoichiometric coefficients for mth component and αth reaction (positive for reagents, negative for products) , W_m – molecular mass of component m, $\beta_{(\alpha)}$ – exponent of temperature for αth reaction , $A_{(\alpha)}$ –'pre-exponential' factor, C_m – molar concentration of reagent component, $\hat{\nu}_{m',(\alpha)}$ – exponent of the concentration of mth reactant in αth reaction, $E_{(\alpha)}$ – activation energy.

3.10   Reaction of methanol decomposition

The main products of the methanol decomposition reaction over Ni_3Al foils are the hydrogen, carbon monoxide and solid carbon deposits. The by-products are carbon dioxide, methane and water. Methanol decomposition may be described by the following equation [7,45]:

$$CH_3OH \ \leftrightarrow CO + 2H_2 \,, \tag{114}$$

$$CO + H_2O \leftrightarrow CO_2 + H_2 \,, \tag{115}$$

$$2CO \ \leftrightarrow C + CO_2 \,, \tag{116}$$

$$CO + 3H_2 \ \leftrightarrow CH_4 + H_2O \,. \tag{117}$$

The type of by-products suggests that the water-gas shift reaction (114), the Boudouard reaction (116) and methanation (117) occur in the performed catalytic test. It is worth noting that some of the by-products, especially water,

can oxidize the Ni_3Al catalyst surface and in effect gradually poison them. It is known from the results presented previously [46] that, H_2O as a by-product of methanol decomposition can be consumed in the reaction, leading to the formation of metallic Ni (118) and then in the subsequent reaction of the production of aluminum hydroxide (119):

$$2Ni_3Al + 3H_2O \leftrightarrow 6Ni + Al_2O_3 + 3H_2 \; , \qquad (118)$$

$$Al_2O_3 + 3H_2O \leftrightarrow 2Al(OH)_3 \; . \qquad (119)$$
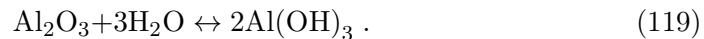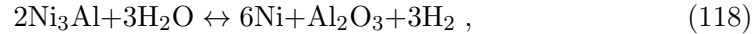
On the other hand, the appearing Ni nanoparticles can also be oxidized by water according to the following reaction (120), and then it can take part in the subsequent reaction of spinel formation (121):

$$Ni + H_2O \leftrightarrow NiO + H_2 \; , \qquad (120)$$

$$NiO + Al_2O_3 \leftrightarrow NiAl_2O_4 \; . \qquad (121)$$

Notwithstanding, the Al_2O_3 formation is energetically privileged and for that preferentially produced on the catalyst surface. According to Moussa *et al.*, the oxidization of Ni_3Al preferentially occurs through grain boundaries [47].

Results obtained on the way of numerical simulations included Eqs. (114)–(115), and (117). However more sophisticated approach including the effects of deposit growth on the reaction conditions (116) and oxidation reaction on the wall (118)–(121) should be considered. To consider chemical reaction, (121), more precise constitutive equations that account for microstructure of solid (porosity factor, tortuosity, and mean grain radii) should be introduced. The appropriate information about material of tested foils was inserted into text (Sec. 4.3).

4   Numerical simulations

Numeric geometry of catalytic microreactor is presented in Fig. 2. In the present analysis a part geometry of a honeycomb set of microchannels has been chosen and zoomed at the left part of Fig. 2. Therefore, four single microchannels with coupling at the ends, located in the middle part of the considered microreactor has been selected for further consideration. The cross section of the channels in the honeycomb set with characteristic dimensions are presented in Fig. 3. In turn, Figs. 4 and 5 show the discretized space flow with visible thickening of the boundary layer. The channel under consideration has been divided into some blocks that have been discretized by means of a structured numerical grid of

finite volume, steeply refined in the normal wall direction. Initial tests allowed to use the numerical grid to ensure that further refinement did not influence the computational results. Microchannels coupling at the ends discretized by means of finite volumes method (FVM) is shown in Fig. 5.
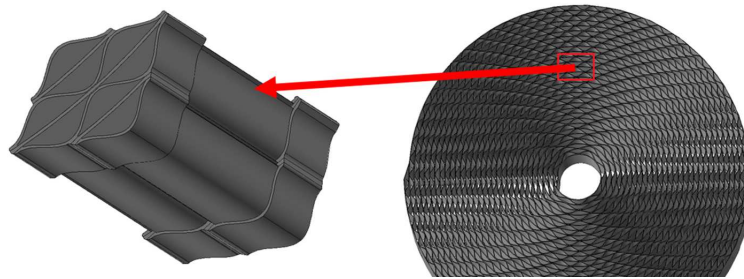
Figure 2: The geometry of four microchannels coupling at the ends taken from the honeycomb.
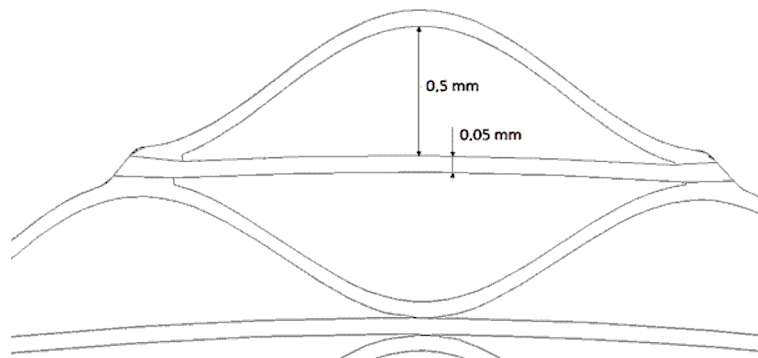
Figure 3: The characteristic dimensions of the microchannels in the honeycomb.

5   Boundary conditions

For calculation, the mass of the catalyst was assumed of 0.777 g. In turn, the normal component of velocity $v_n = \overrightarrow{v} \cdot \overrightarrow{n}$ was assumed at $v_n = 1$ m/s. Additionally, 60% of the mixture is helium and the rest is methanol. It is also known that catalyst temperature is 500 °C.

For the steady state flow analysis a CFD commercial solver was employed. This finite volume based code permits one to solve the three-dimensional fluid and heat flow problems concerned with turbulent structures and chemical reactions.
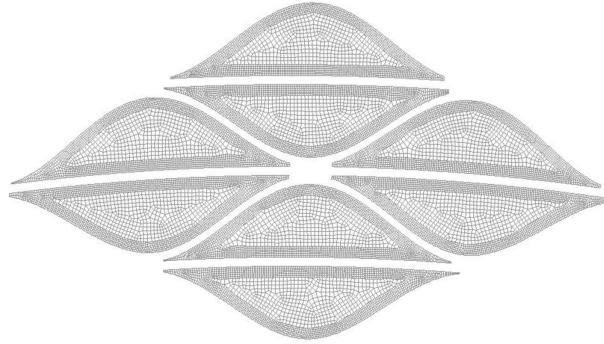
Figure 4: Cross-section through the finite volumes in the four single microchannels, located in the middle part of the considered microreactor.

However, it also allows for the addition of user defined subroutines programmed in C++ for problems that fall outside the capability of the standard version of code.
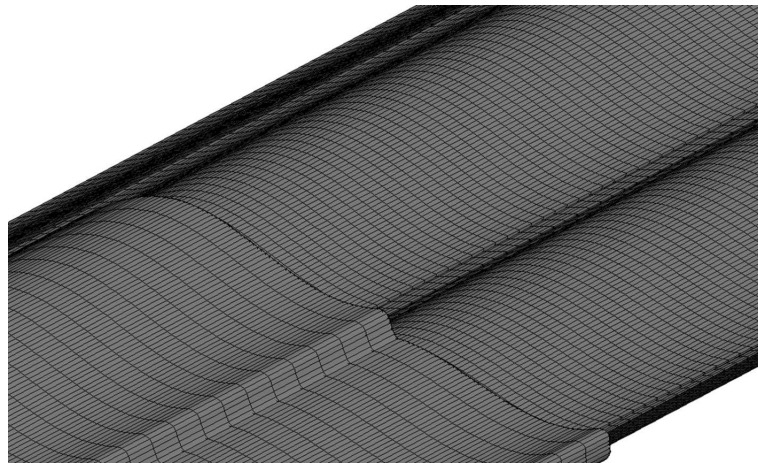
Figure 5: Discretized computing domain – view on coupling of microchannels.

The grid used in the numerical calculations presented here consists of 1 600 000 finite volumes. This allows to maintain high accuracy of the results, without consuming unnecessary computing power. In the microreactor, a k-ε turbulent model was applied due to necessity of usage eddy-dissipation model as easiest one to work on through UDF.

However in this specific case laminar flow has occurred. It was expected due

to several factors: microscale dimensions of the channel, small gas velocity flowing through it and small pressure gradients. Therefore the fundamental dimensionless number related with the integral form of the flow character is the Reynolds number

$$\text{Re} = \frac{v_n \rho d_n}{\mu} = \frac{\dot{m} d_n}{A\mu} = 7.95 \ , \tag{122}$$

which is understood as a dimensionless mass flow rate $\dot{m}$. Here, in a case of complicated cross section we use hydraulic diameter $d_n = 4.22 \times 10^{-4}$ m, at the surface $A = 3.47 \times 10^{-7}$ m^2. Secondly, the viscosity depends on the temperature and pressure and occurs $\mu = 1.72 \times 10^{-5}$ Pa s, for 100 kPa and 500 °C. Additionally, there is assumed $\dot{m}_{in} = \dot{m}_{out} = 1.123 \times 10^{-7}$ kg/s. Hence the Reynolds number can be interpreted as an integral (total) flow parameter. One should remember that in above definition the mass flow rate is defined via normal component of velocity $v_n = \overrightarrow{v} \cdot \overrightarrow{n}$, which ordinary is less than the velocity length $|\overrightarrow{v}| > v_n$.

In contrast, in some special applications, for example, in microfluidic and nanofluidic devices, where the surface-to-volume ratio is huge, the slip velocity behaviour is more typical, and the 'slip' hydrodynamic boundary condition is more often used. Regardless the slip physical mechanism, the degree of slip is normally quantified through the 'slip length', l_s, or a dimensionless slip length (the Navier number) Na [20]. According to the literature previous considerations [17–22] and having in mind the value of the slip length proposed in the literature [48,49], it has been assumed that $l_s = \mu/\nu = 1.6$ μm. This last coefficient ν depends on, both, a kind of fluid and a contacting solid. Thus, the dimensionless slip length (the Navier number) Na equals to

$$\text{Na} = \frac{l_s}{d_n} = 0.0037 \ . \tag{123}$$

Actually, we are in the course of testing of the dimensionless slip length concept. Hence this nonstandard wall function is connected with the boundary condition. But in this work eventually numerical model with no-slip condition (zero velocity at the wall) has been considered. It has been assumed that the microreactor is ideally isolated, thus assures adiabatic condition. It was also assumed that the surface structure of the microreactor can be treated as a homogeneous one.

The standard SIMPLE (semi-implicit method for pressure-linked equations) method has been used for pressure-velocity coupling. The second order upwind schemes have been employed for the solution of the convection term in governing equations. The diffusion terms have been central-differenced with the second order accuracy as well. The detailed methodology of numerical integration regarding the set of governing equations can be found in work [11].

6   Extension of standard code by UDF

Although CFD tools offers models for various cases of combustion (or decomposition of some species) in some instances even wall surface related reactions, there are still unknown reaction rates. In case presented in this paper reaction rates that include the catalyst component Ni_3Al are learned through the experiment conducted specifically for this reason. Prepared UDF code has also another function beside implementing reaction rates corresponding with the experiment. It ensures that catalytic reactions will occur only in cells bordering with walls of the reactor. Moreover it provides results independent from differences in cells volumes appearing during discretisation process using the formula (126) presented below. The idea to model the catalytic reaction in such a manner was previously presented in another work [13]. Concept presented in this work is an extended version of the one featured in the mentioned paper. However the main difficulty which is the proper placement of catalytic reaction is resolved in the same manner as shown in Fig. 6.
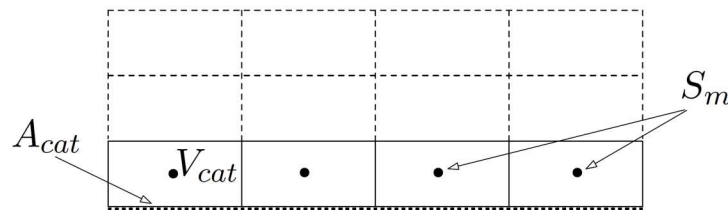
Figure 6: The visual representation of the areas that are directly affected by UDF code concerning catalytic reaction: A_{cat} – surface of active catalytic area, S_m –source of component m, V_{cat} – numerical volume with active catalytic area.

The basic algorithm used in the process of identification cells adjacent to the catalyst surface (as shown in Fig. 6) was presented in the Appendix 1. Moreover the shortened method of recognizing the cell parameters was also included. As a form of protection from false-negative reaction rates values additional measures were taken in the form of 'overwrite_check' variable. The presented UDF is not an entire code used in calculation process but only small part regarding the placement of catalytic reaction (Fig. 6).

The external sources for Ni_3Al can be defined [11,13] as

$$S_m = \sum c_m^+ = \sum W_m \dot{\omega}_m \neq 0 \,, \tag{124}$$

where W_m is the molecular mass of the mth component and $\dot{\omega}_m$ is the molar reaction rate (in moles of substance per cubic meter per second).

The rate of decomposition of the methanol $\dot{\omega}_{\mathrm{CH_3OH}}$ in Eq. (114) depends on catalytic properties of intermetallic phase of $\mathrm{Ni_3Al}$, and the source of $\mathrm{CH_3OH}$ decomposition can be expressed as

$$S_{\mathrm{CH_3OH}} = W_{\mathrm{CH_3OH}}\, \dot{\omega}_{\mathrm{CH_3OH}} = W_{\mathrm{CH_3OH}}\, \nu_{\mathrm{CH_3OH}(\alpha)} q_{(\alpha)}\, , \qquad (125)$$

where total stoichiometric coefficient for methanol equals $\nu_{\mathrm{CH_3OH}\ (\alpha)} = \nu''_{\mathrm{CH_3OH}\ (\alpha)}$ $+\nu'_{\mathrm{CH_3OH}\ (\alpha)}$, while $q_{(\alpha)}$ is the progression level of αth chemical reaction (volumetric reaction rate). To obtain the volumetric reaction rate, $q_{(\alpha)} = q_{\mathrm{CH_3OH}}$ consistent with the volumetric source term $S_{\mathrm{CH_3OH}}$, the surface reaction rate should be divided by the height of the computational cell adjacent to the microreactor wall (A_{cat}/V_{cat}). Therefore, in the case of single surface reactions the source term (103) can finally be rewritten into the form

$$q_{(\alpha)} = q_{\mathrm{CH_3OH}} = k_{cat}[X_{\mathrm{CH_3OH}}]^{\left|\nu'_{\mathrm{CH_3OH}(\alpha)}\right|}$$
$$= k_{cat}[X_{\mathrm{CH_3OH}}]\left(\frac{A_{cat}}{V_{cat}}\right)\, , \qquad (126)$$

where $[X_{\mathrm{CH_3OH}}]$ is the molar concentration of methanol. Hence, the source of $\mathrm{CH_3OH}$ decomposition can be defined as

$$S_{\mathrm{CH_3OH}} = W_{\mathrm{CH_3OH}}\, \nu_{\mathrm{CH_3OH}(\alpha)}\Big[k_{cat}\, [X_{\mathrm{CH_3OH}}]\left(\frac{A_{cat}}{V_{cat}}\right) + c\Big]\, , \qquad (127)$$

where the constant reaction rate c was introduced. This model is valid for atmospheric pressure only under the assumption of a constant temperature in the microreactor of $T = 500\,^{\circ}\mathrm{C}$ for helium/methanol mixture.

Hence, in the paper the 3D numerical analysis of flow with chemical reactionis presented, however, in literature are considered 0D [50,51] and 1D [52] models, which included complicated physicochemical phenomena.

7 Experimental results of decomposition

The model was validated for the stationary parameters of the experiment, mainly from the moment of full decomposition of methanol (Time-on-stream TOS = 270 min), as was shown in Fig. 7. In the examinations the thin $\mathrm{Ni_3Al}$ foils with thickness about 50 μm and average grain size about 15 μm were taken. The stability test for $\mathrm{Ni_3Al}$ catalyst in methanol ($\mathrm{CH_3OH}$) decomposition to hydrogen has been carried out in the fixed-bed plug flow reactor, under atmospheric pressure, at

$500\,°$C. In this case, Ni_3Al foil was placed in the reactor and vapour mixture containing 40%vol. CH_3OH/He was being introduced into reactor (W/F=1.5(g_{cat} s)/cm^3). The desired CH_3OH concentration in the gas phase was obtained by bubbling helium through CH_3OH saturator held at $43\,°$C. The reaction mixture was analysed on-line on TCD-GC (HP 5890 Series II) equipped with Porapak Q packed column. Helium was used as carrier gas in GC. All lines were heated above $100\,°$C in order to prevent water and CH_3OH from condensation. Based on the experiment it has been assumed that constant reaction rate is equal to $c = 2.2$.
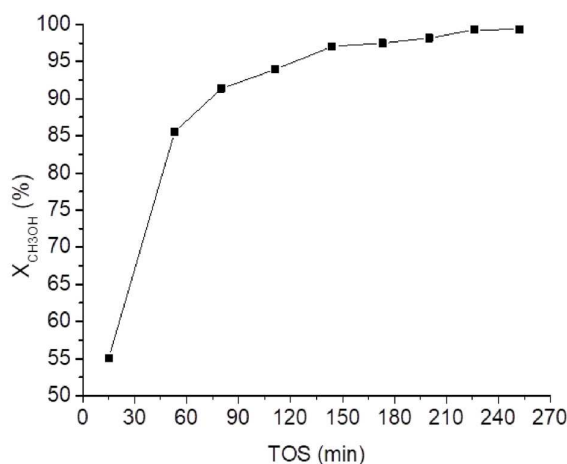
Figure 7: The dependence of the methanol conversion on the reaction time (TOS time-on-stream) for one honeycomb.

There is no proper data for complete model validation, however the full decomposition of methanol occurs, as was in Fig. 7. Partially calibration can be done through the diagram of methanol conversion to the reaction time characteristics that are often available for particular thermocatalytic microreactor. Beside, only scarce data exists for model performance estimation. Specific inlet boundary conditions data are presented in Tab. 1.

The thermocatalytic decomposition rate of methanol q_{CH_3OH} presented in Tab. 1 has been employed for validation purposes. Others parameters have been treated as boundary conditions for CFD calculations.

The most important aspect in a process of validation considered full decomposition of methanol, which has been obtained as well in experiment as in numerical simulation. Additional confirmation for numerical result will be presented in the next section.

Table 1: An experimental thermocatalytic decomposition rate of methanol $q_{\mathrm{CH_3OH}}$ over $\mathrm{Ni_3Al}$ foil estimated at $\dot{Q}_{mix} = 1800$ cm^3/h under the lowest possible temperature of the catalysis process which is sufficient to obtain a full conversion from the initial mole fraction, i.e., $X_{\mathrm{CH_3OH}} = 0.4$.

Parameter	Unit	Value
Total mass of catalytic specimens	g	0.742
Density of Ni$_3$Al foil	g/cm^3	7.51
W/F (weight/flow)	(g$_{cat}$ s)/cm^3	1.5
Conversion of methanol	%	100
Time on stream	h	2
Experimental reaction rate of methanol	g/(g$_{cat}$ s)	1.39

However, the benchmark experiment, which would be in place to check the accuracy along with reliability of proposed supplements, have not been found in the literature by authors. It should be stated that proposed in this work preliminary experiment is accurate to design thermocatalytic reactor.

8 Numerical results

In all tests of catalytic decomposition of methanol, the main product of the reaction is hydrogen and carbon monooxide (see Eq. (114)). Methanol mole fraction distribution at four single microchannels with coupling at the ends is presented in Fig. 8. Methanol mole fraction maximum is located from the beginning of inlet coupling to the A-A cross section, while its lowering due to catalytic reaction in microchannels. Decrease in CH$_3$OH in direction of exit areas is related directly to the decomposition effects due to the properties of intermetallic phase of Ni$_3$Al (see Figs. 9 and 10). The view of the local changes in the field of methanol mole fraction in both the axial-sectional and cross-section is shown in Figs. 8 and 9, respectively.

Examples of the results of turbulent rate of reaction analysis are presented in Fig. 11, which show the zoom in the corner of microchannel with taking into account the state of reaction coming out of the surface of intermetallic phase of Ni$_3$Al and passing through the chamber of microchannels. Hence the view of the local changes in the field of turbulent rate of reaction in cross-sectional was shown in Figs. 10 and 11.
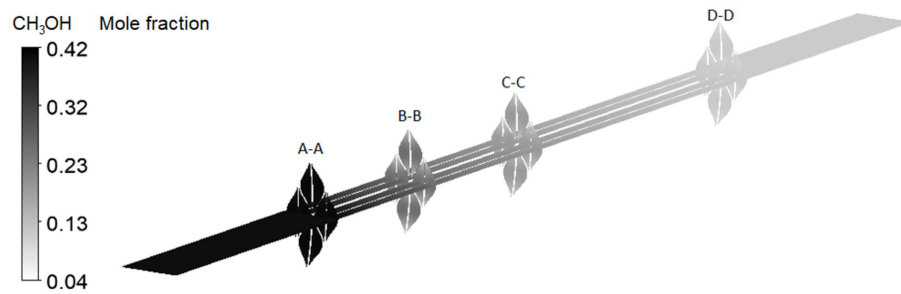
Figure 8: Methanol mole fraction distribution at four single microchannels with coupling.
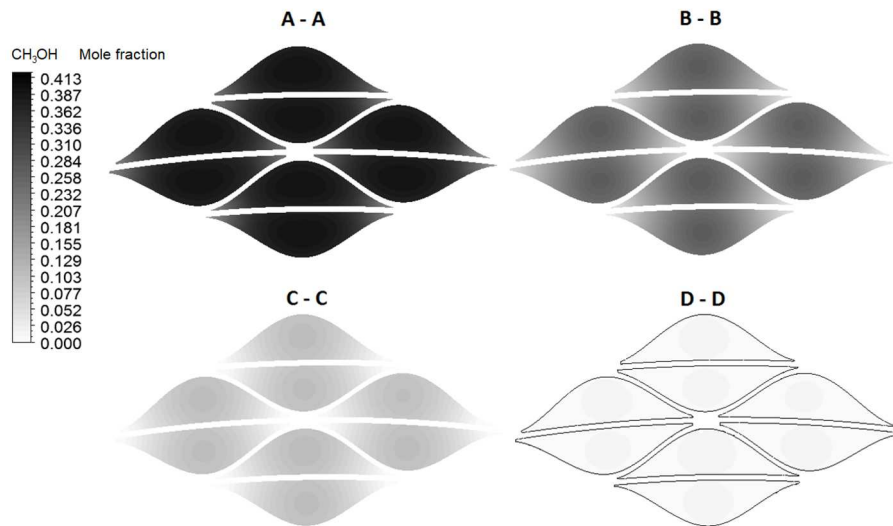
Figure 9: Methanol mole fraction distribution at four single microchannels in the cross section presented in Fig.8, mainly: A-A, B-B, C-C, D-D.

Products of reaction: CO_2, CH_4 (also referred to quantitatively), water and a products of methanol decomposition had a retention time similar to the retention time of methanol. However, at the moment only the 3 main reactions have been modeled (Eqs. (114)–(115), and (117)), and compared with experimental results. Carbon monoxide mole fraction distribution in the cross section D-D and after leaving the reactor domain is shown in Fig. 12. Additionally, the change in molar concentration of methanol, methane, carbon dioxide, carbon monoxide and hydrogen in function of reactor length for two cases, with and without minimum constant reaction rate, has been presented in Fig. 13. Adding the constant
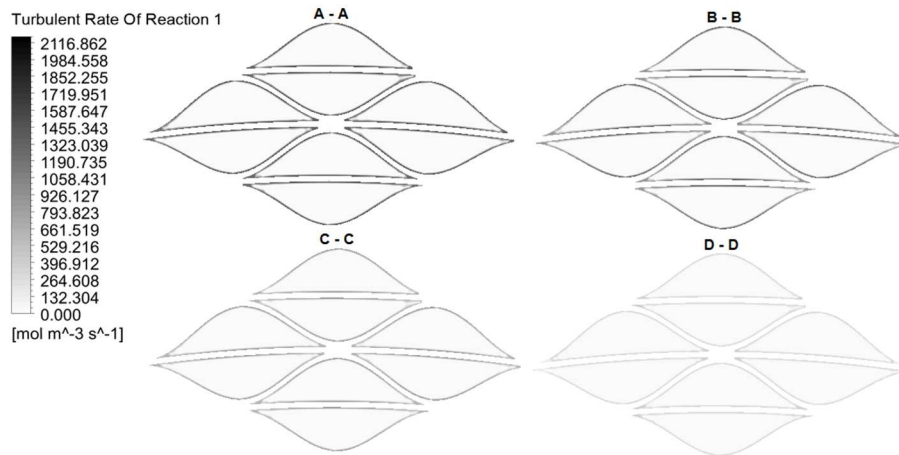
Figure 10: Turbulent rate of reaction at four single microchannels in the cross section presented in Fig. 8, mainly: A-A, B-B, C-C, D-D.
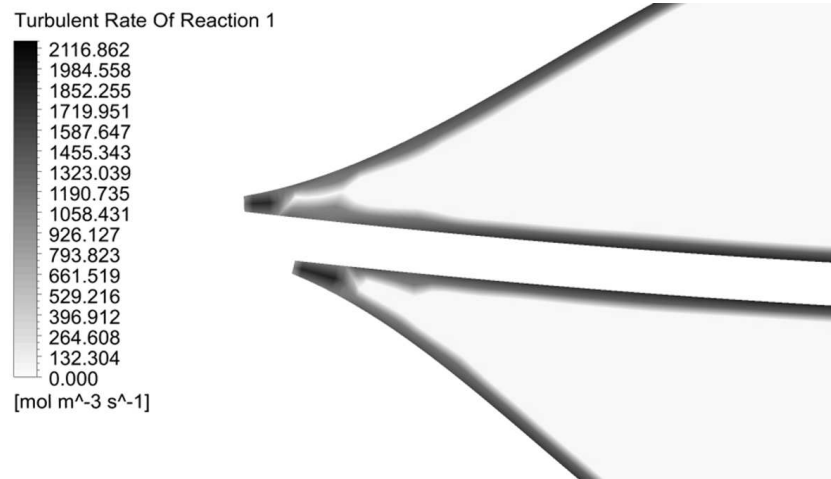
Figure 11: Turbulent rate of reaction at the zoomed microchannels in the cross section A-A.
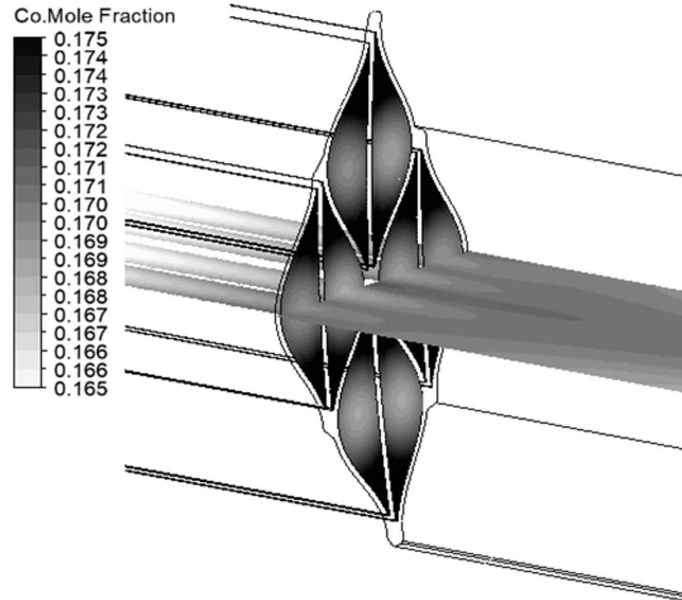
Figure 12: Carbon monoxide mole fraction distribution in the cross section D-D and after leaving the reactor domain.
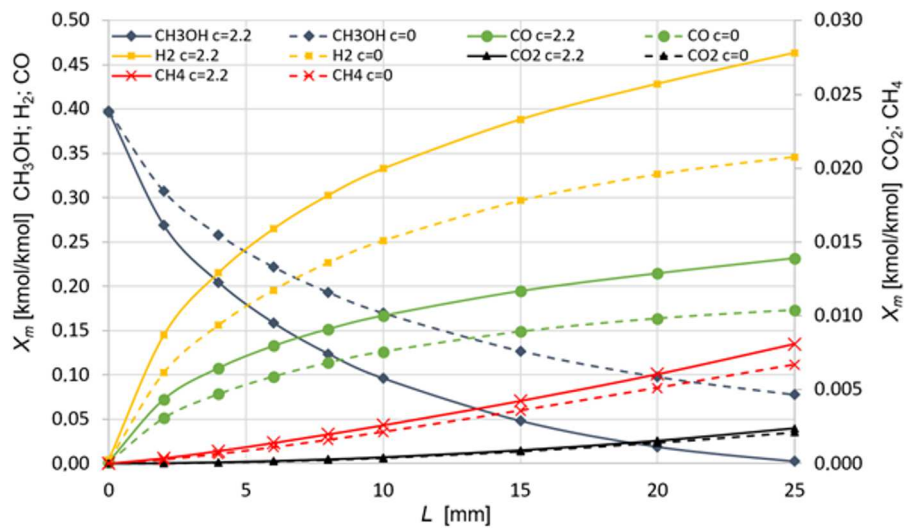
Figure 13: Change in molar concentration of methanol, hydrogen, carbon monoxide, carbon dioxide and methane in function of reactor length for two cases, with (continuous line) and without (dashed line) minimum constant reaction rate.

reaction rate allows to obtain methanol concentration at the outlet below 1%, which is nearly impossible without that constant using Eq. (127).

Longitudinal changes for the mole fraction of methanol, hydrogen, carbon monoxide, carbon dioxide and methane under thermocatalytic decomposition reaction along the investigated microchannel are presented in Fig. 13. The laminar mode of flow limits mass transport towards the wall. In the case of lower volumetric flow rate, there is a sufficient time for every portion of contaminated methanol to be brought from the bulk to the catalytic surface by the molecular diffusion process. In the inlet section of the channel, where reactants concentrations are relatively high and where the still developing velocity profile promotes better mixing near the walls, there is also a more pronounced drop in the methanol mole fraction. In previous paper Jóźwik *et al.* [13] the longitudinal changes of mole fraction reveal a dependency on gas velocity, therefore, thanks to the obtained results and previous experience, it is possible to determine the length of the individual microchannels and whole microreactor.

9   Conclusions

The original methodology of the 3D numerical analysis for thermocatalytic microreactor used in the decomposition of methanol is presented in this paper. The computational fluid dynamic calculations additionally expanded by user defined functions for a mixture containing helium contaminated by methanol flowing in a horizontal microchannels were performed.

In case presented in this paper, data provided as a result of experiment is not sufficient to fully characterize reaction rates of decomposition. Facing that fact the most efficient solution was to take advantage of the possibilities offered by user defined function toolset to fully control not only places where the reaction occur but also to set the reaction rates in such a way, that they cover the limited experiment data as good as possible.

The thermocatalytic decomposition reaction of methanol compound has been modeled through employing some experimental data related to the active surface area. The data extrapolated via the implemented numerical model has made it possible to assess the minimum length of the microreactor channels, which provide an optimal dimension at the system outlet.

intermetallic phase Ni$_3$Al with high activity thermocatalyst in the field of purification of air from harmful substances or controlled decomposition of hydrocarbons'.

Received in May 2017

References

[1] Jóźwik P., Polkowski W., Bojar Z.: *Applications of Ni3Al based intermetallic alloys–current stage and potential perceptivities.* Materials **8**(2015), 2537–2568.

[2] Pohar A., Belaviè D., Dolanc G., Hoèevar S.: *Modeling of methanol decomposition on Pt/CeO2/ZrO2 catalyst in a packed bed microreactor.* J. Power Sources **256**(2014), 80–87.

[3] Grabowski R.: *Kinetics of the oxidative dehydrogenation of propane on vanadia/titania catalysts, pure and doped with rubidium.* Appl. Catal. A: Gen. **270**(2004), 1-2, 37–47.

[4] Riaño J.S.Z., Zea H.R.R.: *Modeling of a microreactor for propylene production by the catalytic dehydrogenation of propane.* Comput. Chem. Eng. **67** (2014), 26–32.

[5] Michalska-Domańska M., Norek M.; Jóźwik P.; Jankiewicz B.; Stępniowski W.J.; Bojar Z.: *Catalytic stability and surface analysis of microcrystalline Ni3Al thin foils in methanol decomposition.* Appl. Surf. Sci. **293** (2014), 169–176.

[6] Michalska-Domańska M., Bystrzycki J., Jankiewicz B., Bojar Z.: *Effect of the grain diameter of Ni-based catalysts on their catalytic properties in the thermocatalytic decomposition of methanol.* C. R. Chimie **20**(2017), 156–163.

[7] Mitani H., Xu Y., Hirano T., Demura M., Tamura R.: *Catalytic properties of Ni-Fe-Mg alloy nanoparticle catalysts for methanol decomposition.* Catalysis Today **281**(2017), 669–676.

[8] Tsoncheva T., Mileva A., Issa G., Dimitrov M., Kovacheva D., Henych J., Scotti N., Kormunda M., Atanasova G., Štengl V.: *Template-assisted hydrothermally obtained titania-ceria composites and their application as catalysts in ethyl acetate oxidation and methanol decomposition with a potential for sustainable environment protection.* Appl. Surf. Sci. **396**(2017), 1289–1302.

[9] Jóźwik P., Grabowski R., Bojar Z.: *Catalytic activity of Ni3Al foils in methanol reforming.* Mater. Sci. Forum **636** (2010), 895–900.

[10] Jóźwik P., Bojar Z., Winiarek P.: *Catalytic activity of Ni3Al foils in decomposition of selected chemical compounds.* Mater. Eng. **3**(2010), 654–657.

[11] Badur J.: *Numerical modeling of sustainable combustion in gas turbines.* Wydawnictwo IMP PAN, Gdańsk, 2003 (in Polish).

[12] Kuo K.K., Acharya R.: *Applications of Turbulent and Multiphase Combustion.* John Wiley & Sons, New Jersey 2012.

[13] Jóźwik P., Badur J., Karcz M.: *Numerical modelling of a microreactor for thermocatalytic decomposition of toxic compounds.* Chem Proc Eng **32**(2011), 3, 215–227.

[14] Aoki N., Yube K., Mae K.: *Fluid segment configuration for improving product yield and selectivity of catalytic surface reactions in microreactors.* Chem. Eng. J. **133**(2007), 105–111.

[15] Karcz M., Badur J.: *An alternative two-equation turbulent heat diffusivity closure.* Int. J. Heat Mass Tran. **48** (2005), 2013-2022.

[16] Karcz M.: *From 0D to 1D modeling of tubular solid oxide fuel cell.* Energ. Convers. Manage. **50**(2009), 2307–2315.

[17] Badur J., Karcz M., Lemański M., Nastałek L., *Foundation of the Navier-Stokes boundary conditions in fluid mechanics.* Trans. Inst. Fluid-Flow Mach. **123**(2011), 3–55.

[18] Badur J., Karcz M., Lemański M.: *On the mass and momentum transport in the Navier-Stokes slip layer.* Microfluid Nanofluid **11**(2011), 439–449.

[19] Badur J., Ziółkowski P.: *Further remarks on the surface vis impressa caused by a fluid-solid contact.* In: Proc. 12th Joint European Thermodynamics Conf. JETC2013 (M. Pilotelli, G.P. Beretta, Eds.), Brescia 2013, 581–586.

[20] Ziółkowski P., Badur J.: *Navier number and transition to turbulence.* J. Physics: Conf. Ser. **530**(2014), 012035. doi:10.1088/1742-6596/530/1/012035.

[21] Badur J., Ziółkowski P.J. Ziółkowski P.: *On the angular velocity slip in nano flows.* Microfluid Nanofluid **19**(2015), 191–198.

[22] Ziółkowski P., Badur J.: *On the unsteady Reynolds thermal transpiration law.* J. Physics: Conf. Ser. **760**(2016), 012041. doi:10.1088/1742-6596/760/1/012041.

[23] Badur J.: *Five lecture of contemporary fluid termomechanics.* Gdańsk 2005, www.imp.gda.pl/fileadmin/doc/o2/z3/.../ 2005_piecwykladow.pdf (in Polish).

[24] Badur J.: *Development of energy concept.* Wyd. IMP PAN, Gdańsk 2009 (in Polish).

[25] Badur J., Banaszkiewicz M.: *Model of the ideal fluid with scalar microstructure. An application to flashing flow of water.* Trans. Inst. Fluid-Flow Mach. **105**(1999), 115–152.

[26] Bilicki Z., Badur J.: *A thermodynamically consistent relaxation model for a turbulent, binary mixture undergoing phase transition.* J. Non-Equil. Thermodyn. **28**(2003), 145–172.

[27] Kornet S., Badur J.: *Enhanced evaporation of the condensate droplets within the asymmetrical shock wave zone.* Trans. Inst. Fluid-Flow Mach. **128**(2015), 119–130.

[28] Lemański M., Karcz M.: *Performance of lignite-syngas operated tubular Solid Oxide Fuell Cell.* Chem. Process Eng. **29**(2008), 233–248.

[29] Linstrom P.J., Mallard W.G. (Eds.): *NIST Chemistry WebBook*, NIST Standard Reference Database Number 69, June 2005, National Institute of Standards and Technology, Gaithersburg MD, 20899 (http://webbook.nist.gov).

[30] Hofman T.: *Termodynamical table for students.* Politechnika Warszawska, Wydział Chemiczny, Warszawa 2008, 2 (in Polish).

[31] Kozaczka J.: *Gasification processes. Engineering methods of calculations.* AGH Kraków, Kraków 1994 (in Polish).

[32] Launder B.E., Spalding D.B.: *Mathematical models of turbulence.* Academic Press, NY, 1972.

[33] Shyy W.: *Computational modeling for fluid flow and interfacial transport.* Dover Pub., NY, 1994.

[34] Wilke C.R.: *A viscosity equation for gas mixtures.* J. Chem. Phys. **18**(1950), 517–575.

[35] Badur J., Feidt M., Ziółkowski P.: *Without heat and work – further remarks on the Gyftopoulos-Beretta exposition of thermodynamics.* Proc. 4th Int. Conf. Contemporary Problems of Thermal Engineering (ISBN 978-83-61506-36-2, W. Stanek, P. Gładysz, L. Czarnowska, K. Petela (Eds), Gliwice-Katowice, 14-16 Sept. 2016, 721–728.

[36] Jou D., Casas-Vazquez J., Criado-Sancho M.: *Thermodynamics of fluid under flow.* Springer, Berlin, 2001.

[37] Hautman D.J., Dryer F.L., Schug K.P. Glassman I.: *A multiple step over kinetic mechanism for oxidation of hydrocarbons.* Combust. Sci. Technology **25**(1981), 219–235.

[38] Badur J., Ziółkowski P., Zakrzewski W., Sławiński D., Kornet S., Kowalczyk T., Hernet J., Piotrowski R., Felicjancik J., Ziółkowski P.J.: *An advanced Thermal–FSI approach to flow heating/cooling.* J. Phys.: Conf. Ser. 530 (2014), 10.1088/1742–6596/530/1/012039.

[39] Ochrymiuk T.: *Numerical prediction of film cooling effectiveness over flat plate using variable turbulent Prandtl number closures.* J. Thermal Science **25**(2016), 3, 280–286.

[40] Williams F.A.: *Combustion theory.* Addision Wesley, Massachussets 1965.

[41] Kuo K.K.: *Principles of combustion.* John Wiley & Sons, New York, 1986.

[42] Dixon-Lewis G.: *Flame structure and flame reaction kinetics, II Transport phenomena in multicomponent systems.* Proc. Roy. Soc. London, A **307**(1968), 111–135.

[43] Shuen J.S., Chen K.H., Choi Y.: *A coupled implicit method for chemical non-equilibrium flows at all speeds.* J. Comp. Phys. **106**(1993), 306–318.

[44] Badur J., Ziółkowski P., Sławiński D., Kornet S.: *An approach for estimation of water wall degradation within pulverized-coal boilers.* Energy **92**(2015), 142–152.

[45] Jang J.H., Xu Y., Chun D.H., Demura M., Wee D.M., Hirano T.: *Effects of steam addition on the spontaneous activation in Ni3Al foil catalysts during methanol decomposition.* J. Molecular Catalysis A: Chemical **307**(2009), 21–28.

[46] Xu Y., Ma Y., Sakurai J., Teraoka Y., Yoshigoe A., Demura M., Hirano T.: *Effect of water vapor and hydrogen treatments on the surfacestructure of Ni3Al foil.* Appl. Surf. Sci. **315**(2014), 475–480.

[47] Moussa S.O., Samy El-Shall M.: *High-temperature characterization of reactively processed nanostructure nickel aluminide intermetallics.* J. Alloys Compd. **440**(2007), 178–188.

[48] Holt J.K., Park, H.G., Wang, Y.M., Stadermann, M., Artyukhin, A.B., Grigoropoulos, C.P., Noy, A., Bakajin, O.: *Fast mass transport through sub–2-nanometer carbon nanotubes.* Science **312**(2006), 5776, 1034–1037.

[49] Whitby M., Cagnon L., Thanou M., Quirke N.: *Enhanced fluid flow through nanoscale carbon pipes.* Nano Lett **8**(2008), 9, 2632–2637.

[50] Lemański M., Badur J.: *Parametrical analysis of a tubular pressurized SOFC.* Arch. Thermodyn. **25**(2004), 1, 53–72.

[51] Kardaś D.: *From biomass towards syngas.* Trans. Inst. Fluid-Flow Mach. **127**(2015), 63–89.

[52] Kardaś D., Polesek-Karczewska S., Ciżmiński P., Stelmach S.: *Prediction of coking dynamics for wet coal charge.* Chem. Process Eng. **36**(2015), 3, 291–303.

Appendix.1: The UDF example implemented into CFD calculation

```
if (C_YI(c, t, 5) > 0.0001) // 5 - methanol
    {
    overwrite_check = 0;
    c_face_loop(c, t, i)
    {
    zn = THREAD_ID(C_FACE_THREAD(c, t, i));
    if ((zn == 39) ) // 39 ID of the reactor walls
    {
    f = C_FACE(c, t, i);
    tf = C_FACE_THREAD(c, t, i);
    F_AREA(A, f, tf);
    area = NV_MAG(A);
    vol = C_VOLUME(c, t);
    density = C_R(c, t);
    m1_fraction = C_YI(c, t, 5);
    Xk = (m1_fraction / Mk_CH3OH) / (m_H2O_fr / 18 + m_CH4_fr
    / 16 + m_H_fraction / 2 + m_CH3OH_fr / 32 + m_CO_fraction
    / 28 + m_C_fr / Mk_C + m_CO2_fr / Mk_CO2 +
    +(1 - m_H2O_fr-m_C_fr-m_CO2_fr - m_CH4_fr - m_H_fraction - m_CH3OH_fr
    - m_CO_fraction) / Mk_He);
    *rate = (mole_stream / V_rector)*Xk*(area/vol) ;
    *rr_t = *rate;
    overwrite_check = 1;
    }
    else if (overwrite_check = 0)
    {
    *rate = 0;
    *rr_t = *rate;
    }
    }
    }
    else
    {
    *rate = 0;
    *rr_t = *rate;
    }
```